www.czasopisma.pan.pl PAN POLSKA AKADEMIA NAUK www.journals.pan.pl

Arch. Metall. Mater., Vol. 61 (2016), No 3, p. 1303–1308

DOI: 10.1515/amm-2016-0215

M. PAWLYTA*#, K. LABISZ*, K. MATUS*

PHASE IDENTIFICATION OF NANOMETRIC PRECIPITATES IN Al-Si-Cu ALUMINUM ALLOY BY HR-STEM INVESTIGATIONS

Aluminium recycling is cost-effective and beneficial for the environment. It is expected that this trend will continue in the future, and even will steadily increase. The consequence of the use of recycled materials is variable and difficult to predict chemical composition. This causes a significant reduction in the production process, since the properties of produced alloy are determined by the microstructure and the presence of precipitates of other phases. For this reason, the type and order of formation of precipitates were systematically investigated in recent decades. These studies involved, however, only the main systems (Al-Cu, Al-Mg-Si, Al-Cu-Mg, Al-Mg-Si-Cu), while more complex systems were not analysed. Even trace amounts of additional elements can significantly affect the alloy microstructure and composition of precipitates formed. This fact is particularly important in the case of new technologies such as laser surface treatment. As a result of extremely high temperature and temperature changes after the laser remelting large amount of precipitates are observed. Precipitates are nanometric in size and have different morphology and chemical composition. A full understanding of the processes that occur during the laser remelting requires their precise but also time effectively phase identification, which due to the diversity and nanometric size, is a major research challenge. This work presents the methodology of identification of nanometer phase precipitates in the alloy AlSi9Cu, based on the simultaneous TEM imaging and chemical composition analysis using the dispersion spectroscopy using the characteristic X-ray. Verification is performed by comparing the simulation unit cell of the identified phase with the experimental high-resolution image.

Keywords: phase identification, precipitates, STEM- HAADF

1. Introduction

In comparison to primary production, less than 10% of energy is used for recycling aluminum [1]. It is not surprising that the share of aluminum which comes from recycling is steadily increasing, and it is expected that this trend will be maintained in the future. After recycling final chemical composition of obtained alloy depend on used products, while properties strongly depend on microstructure and present precipitates. Therefore, the type of precipitates, the sequence in which they occur during the thermal treatment and their influence on the properties of alloys have been extensively studied over the past decades [2-8]. The occurring sequence of the precipitates is predictable based on the value of free energy - the first phase with the lowest free energy is formed, and then after exhausting its constituents locally, another are formed. Sometimes, this sequence is more complicated and at the same time, several different phases could precipitate simultaneously. Previous studies were performed only for the main groups of wrought heat-treatable alloys (Al-Cu, Al-Mg-Si, Al-Cu-Mg, Al-Mg-Si-Cu) (Table 1). More complicated systems have not yet been so far analyzed in detail.

Even trace amounts of additional elements (like Ti, Mn, ...) can significantly affect the microstructure and composition of the emerging precipitates. For that reason, it is important to understand how precipitates influence on the material properties, especially in the case of new technologies like laser surface treatment [9]. As a result, of an extremely high temperature and extremely quick temperature change after laser remelting fine structure with nanometric precipitate are observed. An example is shown in Figure 1. Image shows a section of the sample with a considerable amount of nanometric titanium precipitates. Due to the variety and quantity of visible precipitates, its nanometric size and complex chemical composition, characterization of such materials

TABLE 1

Crystallographic and morphological data of selected phases in aluminum alloy [7]

Alloy system	Equilibrium phase (Bravais lattice)	Metastable phase	
Al - Cu	θ (body centered tetragonal)	θ'	body centered tetragonal (plate)
Al – Mg - Si	B (face centered cubic)	β'	hexagonal (rod)
Al – Cu - Mg	S (side centered orthorhombic)	S'	side centered orthorhombic (lath)
Al – Mg – Si – Cu	Q (hexagonal)	Q'	hexagonal (lath)

* SILESIAN UNIVERSITY OF TECHNOLOGY, INSTITUTE OF ENGINEERING MATERIALS AND BIOMATERIALS, 18A KONARSKIEGO STR., 44-100 GLIWICE, POLAND

Corresponding author: miroslawa.pawlyta@polsl.pl

are challenging. It is recommended to develop simplified procedures which enable precise but sufficiently effective phase identification. The aim of this paper is to describe a methodology for identification of precipitates in aluminum alloy using simultaneous HAADF imaging and EDS analysis.

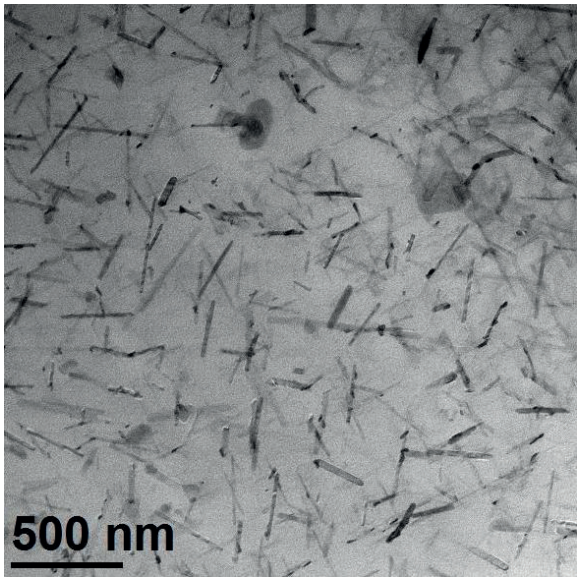

Fig.1. STEM-BF image of AlSi9Cu alloy structure after remelting by the laser beam.

2. Experimental

The investigation has been carried out on AlSi9Cu aluminum alloy (Al – 88 %, Si – 9 %, Cu – 1 %, Fe – 0.7 %, Mn – 0.4%, Mg – 0.3 %). The material was remelted by a laser beam (the high power diode laser HPDL Rofin DL 020, laser power – 1.5 kW, laser scan rate – 0.25 m/s, temperature – up to 3000ºC). The bulk sample was cut into a plate form and then mechanically ground to a thin foil. The specimens for electron microscopy were thinned by ion milling. Electron microscopy observations were done on a probe Cs-corrected S/TEM Titan 80-300 FEI microscope equipped with EDAX EDS detector. The sample was previously oriented in [001] Al direction. The images were recorded in STEM-mode, using the HAADF (High-angle annular dark field) detector. A 300 keV electron beam with a convergence semi-angle of 17 and 27 mrad was used. HAADF is a ring detector that collects electrons scattered at a large angle. At a high angle scattering results from the interaction of electrons with nuclei (the predominant component is the Rutherford scattering), where the differential scattering cross-section I (χ) is proportional to the square of the electric charge of the nucleus (I (χ) ~ Z^2). HAADF detector enables to indicate the contrast between the columns of atoms containing elements of differentiated value Z. Images are obtained by recording the intensity of scattered electrons as a function of incident beam position on the sample surface [10]. For EDS analysis, larger beam current and larger convergence semi-angle (34 mrad) were used to increase the signal. For crystal structure simulations Vesta [11] and Eje-Z [12-13] software were used.

3. Results

The most characteristic feature of the investigated samples after the laser alloying is the presence of areas where densely and evenly distributed precipitates are present. The precipitates are similar in size and shape (Fig. 1a). Most of them are decorated by smaller particles with different Z contrast (chemical composition). Precipitates often have a complex structure, an example of three different phases, marked as Q, β' and θ', is visible in Fig. 2. Figure 3a shows a part (about 6x6 nm) of the precipitate marked as Q. It is characteristic that the distance between the nearest bright spots is constant (approximately 6Å), and their layout resembles honeycomb structure (or currently fashionable graphene). In the center of the hexagon, whose vertices are the bright points is a point of lesser intensity. Precipitate consist of four elements: O, Mg, Al and Si (Fig. 3b).

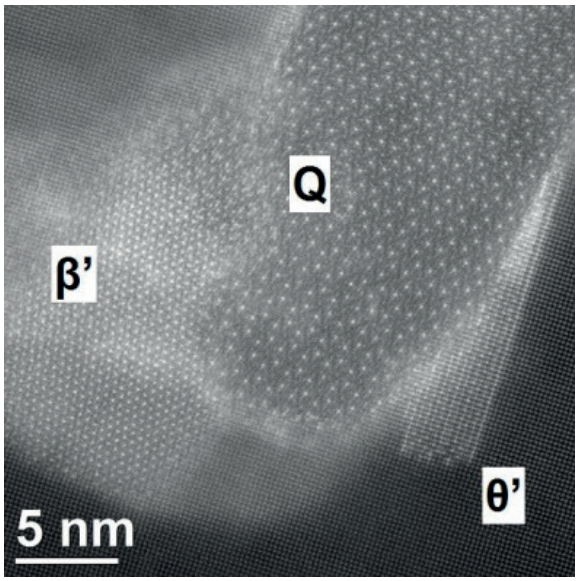

Fig. 2. HAADF image of typical precipitate consisted of three different phases: Q - $Al_3Cu_2Mg_9Si_7$, β' - $Mg_{1.8}$ Si and θ' - Al_2Cu

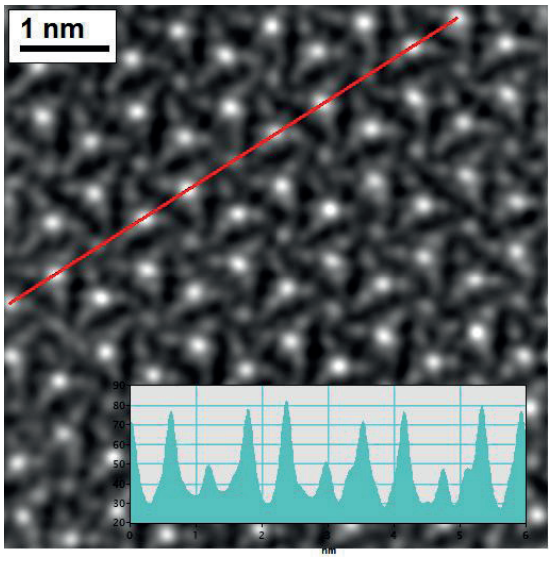

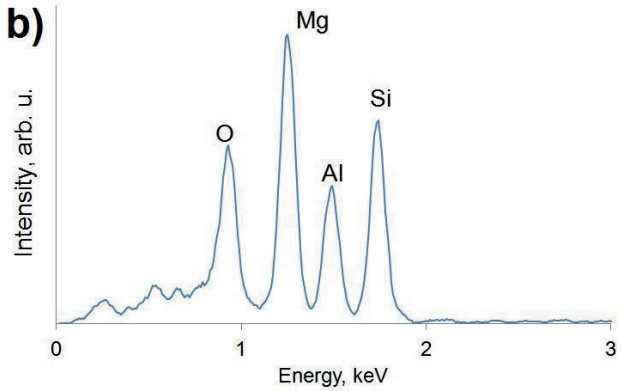

Fig. 3. FFT noise-filtered HAADF image of the Q - Al3Cu2Mg9Si7 (selected part of Fig. 2) with the intensity of the HAADF signal across the profile (red line) (a), EDS spectrum (b).

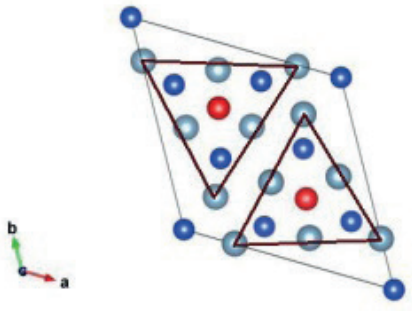

Fig. 4. Crystal structure of Q - Al3Cu2Mg9Si7 [14] viewing along [1 0 0], Cu – red colour, Si – blue color, Al/Mg – gray colour

Even in the case of a complex system of aluminum alloy, potential number of phases is limited and reference crystallographic details are available. In this case, taking into account, the chemical composition most likely is Q ($Al_3Cu_2Mg_9Si_7$) phase [Tab.2] which is common in a wide variety of Al-Cu-Mg-Si alloys [14]. Another tip was hexagonal structure evident in the case of this precipitate. Lattice parameters of Q phase are a = b = 1.032 Å and c = 4.05 Å, space group is P-6. It remains only to check if observed and proposed phase fit them. Orientation between precipitate and matrix is also usually known. According to the [7] (Tab. 1) Q phase precipitates in the orientation [001]Al || [001]Q. Otherwise (if the orientation is not known), it is necessary (at least once) to determine orientation between the matrix and precipitate yourself. The unit cell of the proposed phase is simulated in determined orientation. View of the unit cell Q ($Al_3Cu_2Mg_9Si_7$) in the direction [001] is shown in Figure 4. The distance between Cu atoms in that projection is equal about 6 Å and is close to the distance of the brightest points in the HAADF image. Fitting of Q - $Al_3Cu_2Mg_9Si_7$ simulation to the HAADF image is shown in Figure 5 and allowed the Cu-rich columns indication. Because of interpretable nature of the HAADF images, Q precipitate may easily be distinguished. Our conclusions are consistent with the result of previous investigations of small precipitates in the Al matrix of 6XXX-series aluminum alloys [15].

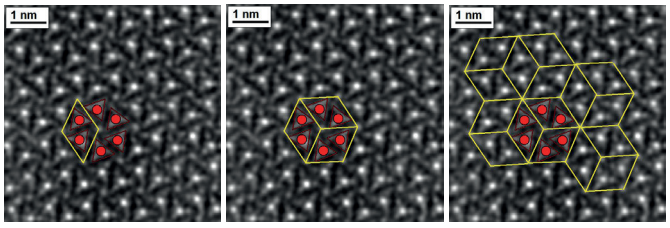

Fig. 5. Fitting of Q - $Al_3Cu_2Mg_9Si_7$ simulation to the HAADF image (Fig. 3a).

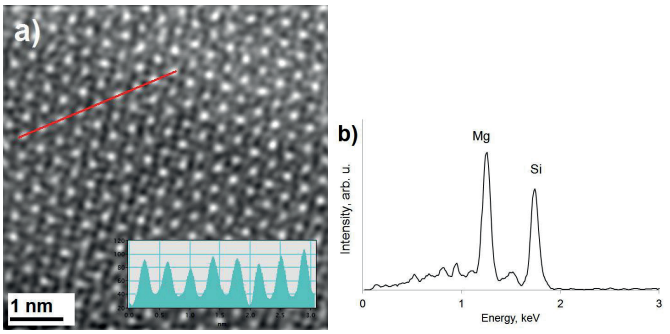

Fig. 6. FFT noise-filtered HAADF image of the β' - Mg1.8 Si (selected part of Fig. 2) with the intensity of the HAADF signal across the profile (red line) (a), EDS spectrum (b).

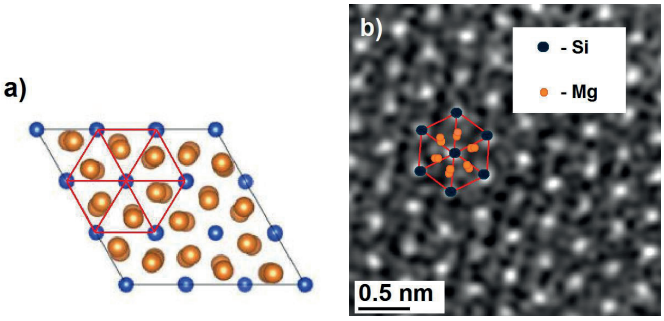

Fig. 7. Crystal structure of β' - Mg1.8 Si [22], viewing along [1 0 0] (a), fitting of β' (Mg1.8 Si) simulation to the HAADF image (Fig. 6a)

TABLE 2

Crystallographic details of observed phases

Precipitate	Crystal structure	Lattice parameters, Å	Space group	Reference
θ' – Al_2Cu	Tetragonal	a=b=4.06 c=7.80	P4/m	[17]
Q – $Al_3Cu_2Mg_9Si_7$	Hexagonal	a=b=1.032 c=4.05	P-6	[14]
β' - $Mg_{1.8}$ Si	Hexagonal	a=b=12.41 c=12.34	P63	[22]
U1 - $MgAl_2Si_2$	Trigonal	a=b=4.05, c=6.74	P-3m1	[20]

Hexagonal structure is also visible in second part of the precipitate, marked as β' in Figure 2. The enlarged part is shown in Figure 6a. The distance between points forming a hexagonal network is approximately constant (about 4 Å), and their intensities are similar (inset in Fig. 6a). Precipitate consist on Mg and Si (Fig. 6b). Potential phase is β'- $Mg_{1.8}Si$ (Table 2) – present (for example) in Al–Mg–Si alloys containing Cu and transition metals [16]. Crystal structure of proposed phase is presented in Figure 7 (view in [001]). Seven of Si atoms are bonded by the red lines, creating a distinctive shape (hexagon of six isosceles triangles). The same pattern is indicated on magnified image (Fig. 7b), were fitting of β' simulation to the HAADF image is presented.

The third part of the precipitate from Fig. 2 has a longitudinal shape (width of about 2 nm and a length of about 5 nm, the magnified image is shown in fig. 8a). Precipitate consist on Cu and Al (Fig. 8b). Potential phase is θ'- Al_2Cu (Tab. 2, [17]). The view of this phase in the [001] direction and fitting to the HAADF image is shown in Figure 9. Similar HAADF-STEM image of that precipitate acquired along [001] direction can be found in [18]. Co-precipitation of θ′- and Q-phase precipitates was described in [19]. A combination of atom-probe tomography (APT), differential scanning calorimetry (DSC), transmission electron-microscopy, X-ray diffraction and first-principles calculations was employed to reveal the compositional evolution of Q-phase precipitates in a commercial, age-hardenable aluminum alloy, W319. Obtained results suggested that Q-phase precipitates serve as heterogeneous nucleation sites for θ′-platelets. In fig. 2 and in fig. 12b it is directly confirmed.

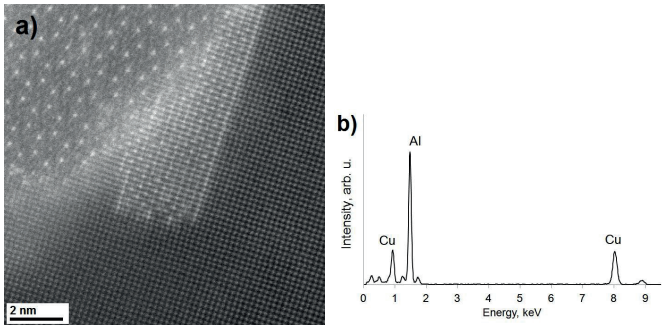

Fig. 8. HAADF image of the θ' - Al_2Cu (selected part of Fig. 2) (a), EDS spectrum (b)

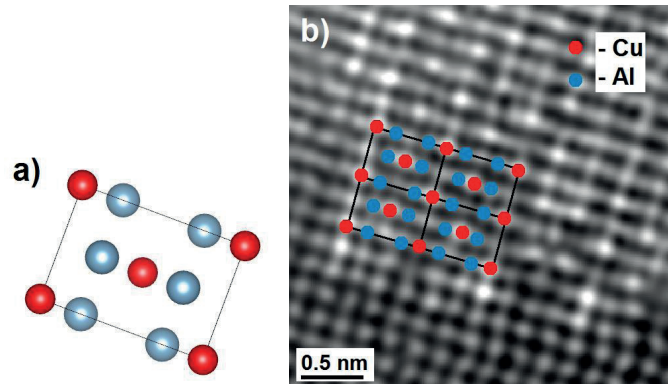

Fig. 9. Crystal structure of θ' - Al_2Cu [17], viewing along [1 0 0] (a), fitting to the HAADF image (enlarged part from Fig. 8a)

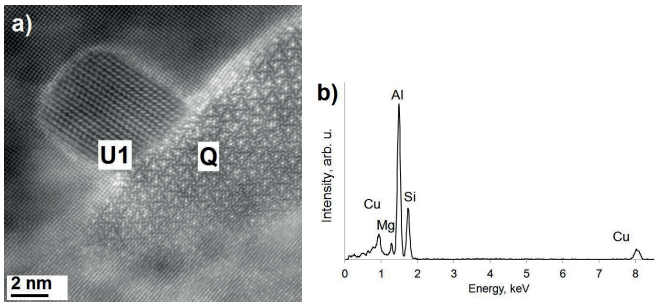

Fig. 10. HAADF image of the U1 and Q precipitate in the α-Al matrix (a), EDS spectrum of U1 precipitate (b).

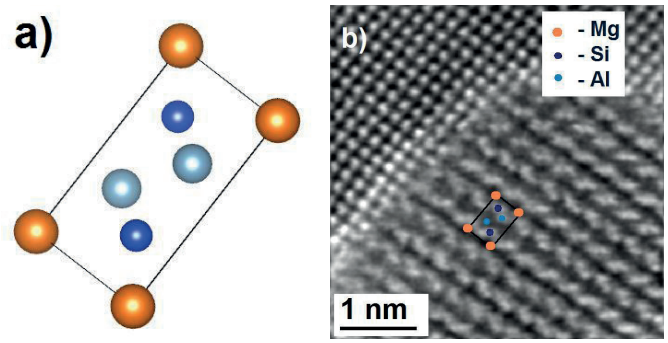

Fig. 11. Crystal structure of U1 - $MgAl_2Si_2$ [20], viewing along [-1 0 0] (a), fitting to the HAADF image (enlarged part from Fig. 10a)

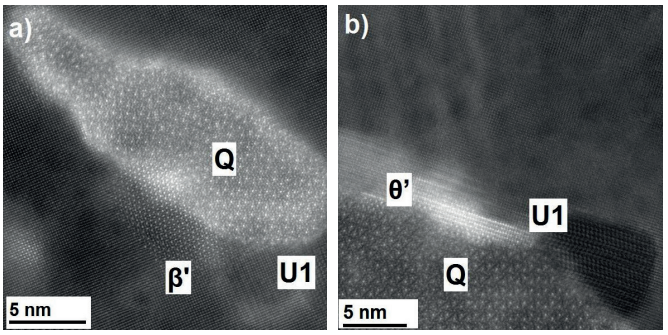

Fig. 12. Two examples of complex precipitates consisted of a mixture of θ', U1, Q and/or β'

Another phase frequently found in our sample is U1. An example of that precipitate is shown in Fig. 10a. Precipitate consist on Al, Si, Mg (Fig. 10b) (the presence of Cu is not clear, it is probably an artifact while the Al content may be overstated and come up from the matrix). We assumed that it is U1-$MgAl_2Si_2$ (Tab. 2, [20]). That phase was previously described as the main precipitate types in 6xxx Al-Mg-Si alloys with large Si/Mg=2 ratio (total solute content was 1.3 at%) [21]. The view of this phase in the [001] direction and fitting to the HAADF image is shown in Figure 11.

Figure 12 presents two more examples of complex precipitates in the alloy under consideration. By morphology and (in the case of doubt) chemical analysis, it was possible to identify precipitates which were earlier described in detail.

4. Conclusions

The structure of an aluminum alloy after laser treatment was investigated. The area containing numerous, similar

in size, shape, and chemical composition precipitates were observed. Four types of precipitates (θ', β', Q, and U1) coexisting in an over-aged state were found. All of them are common for Al–Mg–Si–Cu system [7, 21] Observed precipitates with [001]Al coherencies nucleated mainly on needle precipitates (Ti), while no precipitates were found on round Mn precipitates. Phases of nanometric precipitates were identified by complementary using scanning transmission electron microscopy (HAADF imaging) and energy-dispersive X-ray spectroscopy.

Acknowledgement

This publication was financed by the Ministry of Science and Higher Education of Poland as the statutory financial grant of the Faculty of Mechanical Engineering SUT.

REFERENCE

[1] M.E. Schlesinger, Aluminum recycling. CRC Press 2013.
[2] E. Sjölander, S. Seifeddine, J Mater Process Tech. **210**, (10), 1249-1259 (2010).
[3] H. W. Zandbergen, S. J. Andersen, J. Jansen, Science. **277**, (5330), 1221-1225 (1997).
[4] H.S. Hasting, A.G. Frøseth, S.J. Andersen, R. Vissers, J.C. Walmsley, C.D. Marioara, R. Holmestad, J Appl Phys. **106**, (12), 123527 (2009).
[5] C. Ravi, C. Wolverton, Acta Mater. **52**,(14), 4213-4227 (2004).
[6] K. Matsuda, S. Ikeno, Y. Uetani, T. Sato, Metall Mater Trans A. **32**,(6), 1293-1299 (2001).
[7] D.J. Chakrabarti, D.E. Laughlin, Prog Mater Sci. **49**,(3), 389-410 (2004).
[8] S.P. Ringer, K. Hono, K. Mater Charact. **44**,(1), 101-131 (2000).
[9] K.G. Watkins, M.A. McMahon, W.M. Steen, Mat Sci Eng A-Struct. **231**,(1), 55-61(1997).
[10] R. Brydson: Aberration-corrected Analytical Transmission Electron Microscopy. John Wiley and Sons, Chichester (2011).
[11] K. Momma, F. Izumi, "VESTA 3 for three-dimensional visualization of crystal, volumetric and morphology data," J. Appl. Crystallogr. **44**, 1272-1276 (2011).
[12] J.A. Perez-Omil, PhD Thesis (1994) University of Cadiz – Spain.
[13] S. Bernal, F.J. Botana, J.J. Calvino, C. Lopez-Cartes, J.A. Perez-Omil, J.M. Rodrıguez-Izquierdo, Ultramicroscopy **72**, (3), 135-164 (1998).
[14] C. Wolverton, Acta Mater **49**, (16), 3129-3142 (2001).
[15] H. S. Hasting, J.C. Walmsley, A.T.J. Van Helvoort,C.D. Marioara, S.J. Andersen, R. Holmestad, R., Phil Mag Lett **86**(9), 589-597 (2006).
[16] K. Matsuda, S. Taniguchi, K. Kido, Y. Uetani, S. Ikeno, Mater Trans **43**(11), 2789-2795 (2002).
[17] L. Bourgeois, C. Dwyer, M.Weyland, J.F. Nie, B.C. Muddle, Acta Mater **60**,(2), 633-644 (2012).
[18] S. Wenner, C.D. Marioara, S.J.Andersen, M. Ervik, R. Holmestad, Mater Charact, **106**, 226-231 (2015).
[19] A. Biswas, S.J. Siegel, D.N. Seidman, Acta Mater, **75**, 322-336 (2014).
[20] S.J. Andersen, C.D. Marioara, R. Vissers, A. Frøseth, H.W. Zandbergen, Mat Sci Eng A-Struct. **444**,(1), 157-169. (2007).
[21] C.D. Marioara, H. Nordmark, S.J. Andersen, R. Holmestad, J Mater Sci **41**(2), 471-478 (2006).
[22] S. Ji, M. Imai, H. Zhu, S. Yamanaka, Inorg. Chem. **52**, 3953-3961 (2013).